Journal of Catalysis 287 (2012) 93–101

Contents lists available at SciVerse ScienceDirect

Journal of Catalysis

journal homepage: www.elsevier.com/locate/jcat

Variation of residence time with chain length for products in a slurry-phase Fischer–Tropsch reactor

Cornelius Mduduzi Masuku [a,b,*], Wilson Davis Shafer [a], Wenping Ma [a], Muthu Kumaran Gnanamani [a], Gary Jacobs [a], Diane Hildebrandt [b], David Glasser [b], Burtron H. Davis [a]

[a] Center for Applied Energy Research, University of Kentucky, 2540 Research Park Drive, Lexington, KY 40511, USA
[b] Centre of Materials and Process Synthesis, University of the Witwatersrand, Private Bag 3, WITS 2050, South Africa

ARTICLE INFO

Article history:
Received 11 August 2011
Revised 29 November 2011
Accepted 2 December 2011
Available online 29 December 2011

Keywords:
Hydrocarbons residence time
Deuterium tracer
Vapor–liquid equilibrium
Fischer–Tropsch product accumulation
Chain length–related phenomena

ABSTRACT

The phrases "product accumulation" or "accumulated products" or "product holdup" have appeared in literature during the past several decades to qualitatively explain the experimental results for Fischer–Tropsch synthesis (FTS). This study develops an experimental method for a slurry reactor to evaluate the product accumulation inside the FT reactor by measuring the average residence time of products as a function of carbon number. The effect of accumulation of products on vapor–liquid equilibrium (VLE) in the reactor is also investigated. The results show that VLE is reached inside the FT reactor for components up to C_{17}. Furthermore, the relationship between the mole fractions of components in the vapor and the liquid phase for lighter hydrocarbons, up to around C_{17}, is adequately described by Raoult's law. These results suggests that chain length–dependent solubility in the liquid phase is the predominant cause for chain length dependencies of secondary olefin reactions in FTS, and diffusion-limited removal of products is only significant for products with carbon number greater than 17.

1. Introduction

The chemical industry faces unparalleled challenges, in terms of providing for growing energy markets and meeting the needs of an increasing world population that aspires to a more advanced material quality of life, while simultaneously minimizing the environmental impacts of pollution from the process industry. The world's resources are limited, particularly crude oil and the other fossil fuels, and hence, an improvement in the efficiency of chemical manufacture is required to increase product yields, improve selectivities, and reduce energy costs. The Fischer–Tropsch synthesis (FTS) reaction is an area that is receiving revived interest worldwide as a technology alternative to produce both transportation fuels and chemicals from synthesis gas (syngas). FTS has been studied for over 80 years [1]. FTS produces a range of hydrocarbons of different chain lengths, and based on the product analysis, Friedel and Anderson [2] in the 1950s found that the products obtained during synthesis followed an Anderson–Schulz–Flory (ASF) distribution as shown in the following equation:

$$m_n(1-\alpha)\alpha^{n-1} \quad (1)$$

where n is the number of carbon atoms in the hydrocarbon, m_n is the mole fraction of products containing n carbon atoms, and α is the probability of chain growth. Around the same period, Emmett and coworkers [3–5] found that the C_2 species derived from ethanol or ethylene acted as an initiator for the FTS reaction. This conclusion was based on the observation that the molar radioactivity of hydrocarbons from C_3 to about C_8 is the same when ^{14}C-labeled ethanol or ethylene was used as tracers. The ASF distribution equation and the conclusions obtained from ^{14}C tracer studies provided the bases for understanding the mechanism of the FTS reaction.

However, subsequent studies showed that the measured product distribution from the FTS reactions seldom obeyed the ASF kinetics, especially when the carbon number of the hydrocarbons was greater than around 8, leading to either negative [6–9] or positive deviations [10–15] from the ASF distribution; the measured α values increase with decreasing syngas flow rate [14,16]; the paraffin-to-olefin ratio increases exponentially with increasing the molecular size [17], and the molar radioactivity or stable isotope content of hydrocarbons decrease with increasing molecular size for an initiator [18–21].

To explain these chain length–related phenomena, theories proposed include: models based on the assumption of two-active-sites [12,13], models based on diffusion-enhanced olefin readsorption effects [14,22,23], olefin readsorption product distribution models [24], models based on the different physisorption strength of the olefins [15–17], or the greater solubility of larger olefins [16,17],

* Corresponding author at: Centre of Materials and Process Synthesis, University of the Witwatersrand, Private Bag 3, WITS 2050, South Africa. Fax: +27 11 717 7557.
E-mail address: Cornelius.Masuku@students.wits.ac.za (C.M. Masuku).

0021-9517/$ - see front matter © 2011 Elsevier Inc. All rights reserved.
doi:10.1016/j.jcat.2011.12.005

and VLE phenomena–based models [9,25,26]. Some of the theories proposed over the past several decades can address some of the observed chain length–related anomalies, but none of them can describe all the observations.

Based on the studies of accumulated products in FTS reactions conducted in a continuously stirred autoclave slurry reactor, Shi and Davis [27] proposed that the apparent products of the FTS reaction are a mixture of freshly produced FTS products and the products left in the reactor. Using this concept, most of the chain length–related anomalies were accounted for. According to their model, they concluded that in order to obtain the correct product distribution and the paraffin to olefin ratio of an FTS reaction, it is necessary to find a way to eliminate or evaluate products left in the reactor, which requires conducting FTS research in a different way. However, they did not quantitatively determine the residence times of various hydrocarbons in the FT reactor. In this study, we experimentally measure the residence times of heavier hydrocarbons in the FT slurry reactor and discusses the implications of the results on the modeling of the product distribution. We believe that these observations contribute fundamentally to the understanding of the complex Fischer–Tropsch kinetic regime.

2. Deuterium tracer experiments

In studying the mechanism of FTS, isotopic tracer techniques have been widely used, and based on the results, several very important conclusions have been reported [4,5,28–33]. The most frequently used isotopes in FT reactions are carbon-14- and carbon-13-labeled compounds. Almost all of the possible carbon-14- and carbon-13-labeled compounds suitable for studying the mechanism of FT reactions, such as alcohols, alkenes, CO, CO_2, aldehyde, and many others, have been used as probes [34]. Compared with the number of carbon-14 and carbon-13 tracer experiments, very few deuterium tracer experiments have been conducted to study the mechanism of the FT reaction [35].

Recently, Shi and Davis [36] reported that product holdup has a very important impact on the data interpretation in isotopic tracer studies of FT reactions. They reported that due to the nature of isotope tracer experiments in FTS, this product accumulation factor could be minimized, but could not be removed completely in ^{14}C tracer studies.

The belief that H/D exchange might occur under FT reaction conditions is the main reason why just a few deuterium tracer experiments have been conducted even though the deuterium tracer technique is one of the most frequently used methods in homogeneous organic reactions [32]. However, until recently, no experiment had been performed to show whether there is an H/D exchange reaction among the major products under FT reaction conditions. The importance of this is that if there is no H/D exchange in alkanes, it would be possible to study the chemical behavior of alkanes under FT reaction conditions using the deuterated alkane as the probe.

Shi et al. [35] addressed the questions of whether there is H/D exchange in alkanes under the iron-catalyzed FT reaction conditions and the extent of isomerization of 1-alkene products. They found that deuterium/hydrogen exchange does not occur in alkanes under reaction conditions. Since there was no H/D exchange in the alkane, the opportunity to use deuterium tracer techniques to study the mechanism for FT reaction is appropriate.

3. Experimental section

3.1. FT Reactor and analysis of products

The FT reaction is carried out in a slurry-phase 1-L CSTR autoclave reactor as shown in Fig. 1. CO and H_2 are metered separately and premixed in a 0.5-L vessel before being fed to the reactor. The vapor-phase products exit the reactor out the top of the reactor and pass through a fritted filter and then through two traps in series. The warm trap is maintained at 100 °C, while the cold trap is maintained at 0 °C. The uncondensed gases from these two traps pass through a back-pressure regulator to a flow meter to measure the exit gas flow rate. The uncondensed gases are periodically sampled and analyzed by on-line gas chromatographs (GCs). The condensed products from the warm and cold traps are collected as required and analyzed through offline GCs. The liquid-phase product is collected as required through the internal filter into the hot trap maintained at 200 °C.

A cobalt catalyst on alumina (25% Co/Al_2O_3) with 0.5% Pt was used. 8.3 g of calcined catalyst was reduced ex situ in a plug flow reactor using 25% H_2/He mixture at 350 °C for 10 h. The reduced catalyst was transferred to the 1 L CSTR which already contained 310 g of melted Polywax 3000 (polyethylene with average MW of 200) as a start-up solvent under flowing nitrogen. The catalyst was further reduced in situ using pure H_2 (15 slph) for 24 h at 230 °C. The FT synthesis reaction was conducted at 220 °C, 2.0 MPa with a space velocity of 4.0 slph/g_cat and at a constant H_2/CO ratio of 2.0.

The composition of the uncondensed product gases is obtained from a Hewlett–Packard Quad Series Micro GC, specifically used as a refinery gas analyzer (RGA). The micro GC has four columns that run in parallel. This is used to quickly obtain the mole fractions of CO, H_2, N_2, CO_2, and C_1 to C_6 hydrocarbons in the uncondensed product gases.

The condensed liquid products are separated into an aqueous and a hydrocarbon (oil + wax) phase. The aqueous phase is analyzed in a Hewlett–Packard 5790A gas chromatograph with a Porapak Q packed column using a thermal conductivity detector (TCD). The oil phase is analyzed using a 6890 Agilent GC with a DB-5 capillary column and a flame ionization detector (FID). The wax phase is analyzed using 6890 Agilent GC FID with a high-temperature DB-1 capillary column.

3.2. Analysis of accumulated products

Applications of isotopic tracer techniques have played important roles in developing and understanding of the mechanism for FTS [28]. The general procedure for determining the accumulated products in FTS is as follows: (1) the FTS is started in the 1-L CSTR using H_2/CO as the synthesis gas as described above; (2) after several days, when the reaction has reached a stable CO conversion and/or at the point where the accumulation is to be evaluated, all the collection vessels are emptied and the feed is switched from CO/H_2 to CO/D_2 for 24 h and then switched back to CO/H_2; and (3) a sample is collected every 24 h until deuterium-containing compounds cannot be detected. Likewise, the reaction can also be started by using CO/D_2 as the reagents and then switch to CO/H_2. The deuterium content of the tracer compounds and its products was determined using GC–MS. The quantitative analysis of the isotopomers of products by GC–MS method has been described previously [35].

4. Estimation of the residence time of the gas phase

Hydrogen and deuterium have different thermal conductivities. Hence, the TCD response was used as a quick measure to determine how long it takes to replace H_2 with D_2 in the gas phase as a measure of the residence time in the gas phase. The TCD response shows that in the gas phase, hydrogen is replaced by deuterium within 6 h as shown in Fig. 2.

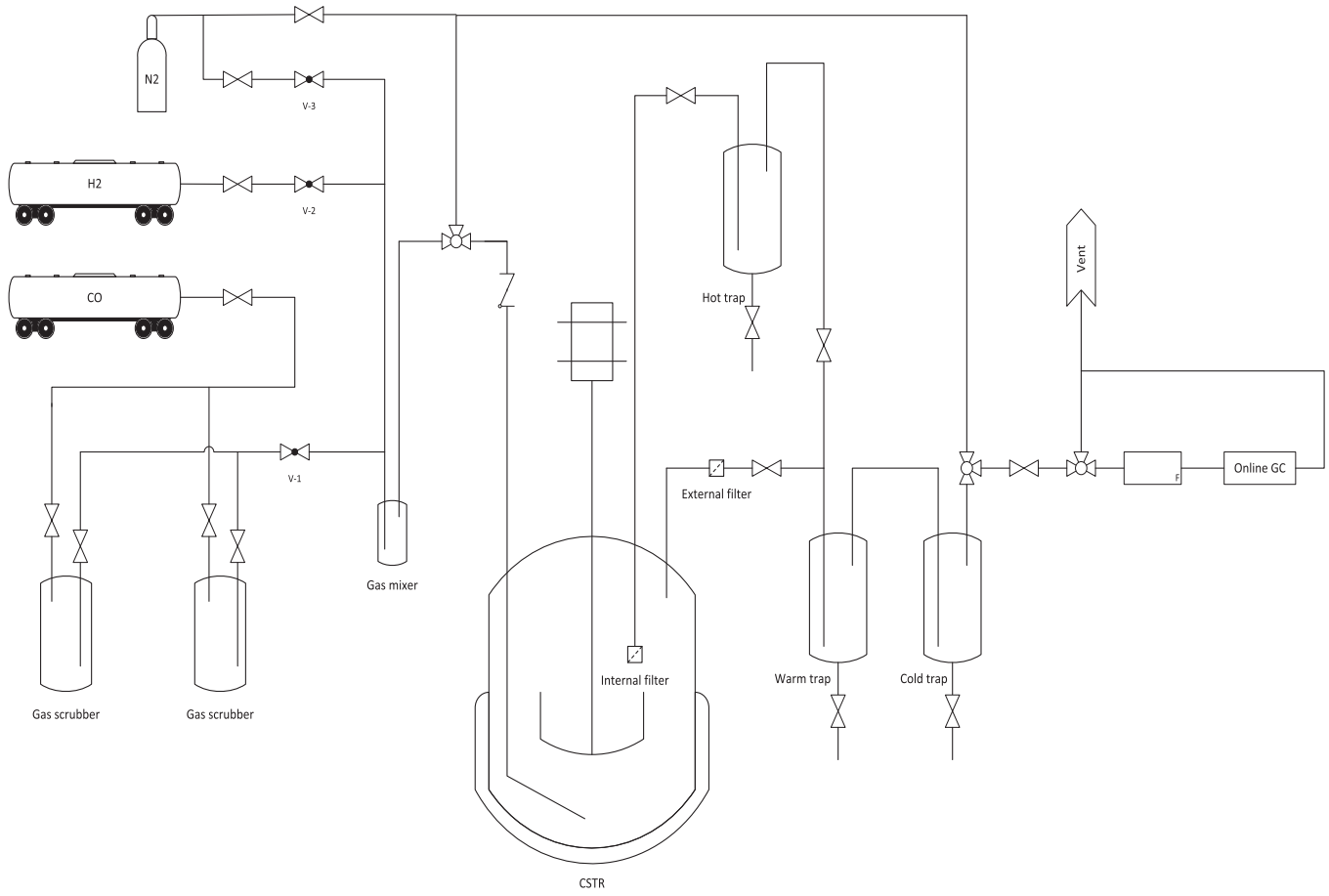

Fig. 1. A schematic diagram of the Fischer–Tropsch reactor system.

After the feed gas has been changed from CO/H_2 to CO/D_2, part of the hydrogen inside the reactor continues reacting while some of it is removed with the gas flowing out of the reactor. The residence time of hydrogen would give a good indication of the gas-phase residence time even though hydrogen is reacting.

If we neglect the effects of reaction and the amount of hydrogen dissolved in the liquid phase, then the unsteady state mass balance becomes:

$$y_{H2} V_G C_G|_t = y_{H2} V_G C_G|_{t+\Delta t} + y_{H2} Q_G C_G \Delta t \tag{2}$$

where V_G is the volume of gas/vapor inside the reactor; C_G, the molar concentration of the vapor inside the reactor; Q_G, the molar flow rate of vapor out of the reactor; and y_{H2} is the mole fraction of hydrogen in the vapor phase.

Therefore, the unsteady state mass balance can be reduced to

$$V_G C_G \frac{dy_{H2}}{dt} = -Q_G C_G y_{H2} \tag{3}$$

The average gas residence time is defined as:

$$\tau_G \equiv \frac{V_G}{Q_G} \tag{4}$$

Substituting the residence time into Eq. (3) gives

$$\frac{dy_{H2}}{dt} = -\frac{1}{\tau_G} y_{H2} \tag{5}$$

which simplifies to:

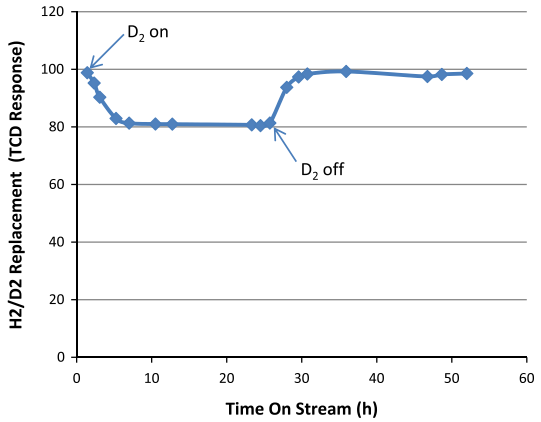

Fig. 2. Measurement of hydrogen–deuterium replacement in the gas phase as indicated by the TCD response as a function of time.

$$\ln\left(\frac{y_{H2}}{y_{H2,0}}\right) = -\frac{1}{\tau_G}(t - t_0) \tag{6}$$

Therefore, Eq. (6) shows that plotting the log of the mole fractions of hydrogen in the reactor versus time on stream should result in a straight line in which the slope is given by $-1/\tau_G$. Using the data in Fig. 2, the mole fraction of hydrogen was calculated, and the results for a short period after switching from CO/H_2 to CO/D_2 are presented in Fig. 3.

As expected, the log of the mole fractions of hydrogen in the reactor versus time on stream is a straight line. The slope of the

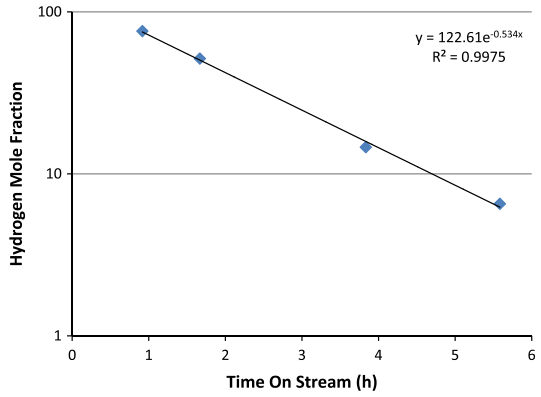

Fig. 3. Logarithm of the mole fraction of hydrogen after switching from CO/H_2 to CO/D_2. Time = 0 is when H_2 is replaced by D_2 in the feed.

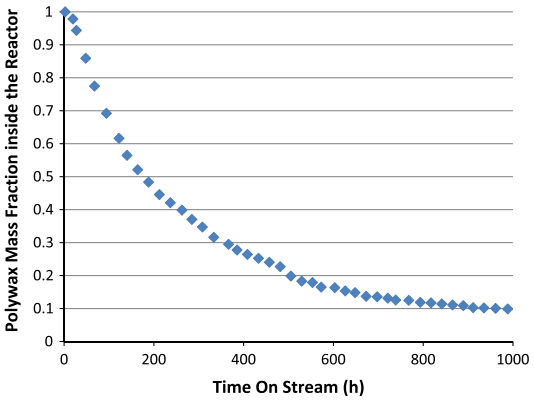

Fig. 4. Calculated polywax mass fraction inside the reactor as a function of time. Time = 0 corresponds to start-up of the reactor.

trend line is −0.534, which results in the average gas-phase residence time of 1.87 h. This estimates the residence time of highly-volatile/insoluble components.

5. Measurement of residence time of polywax in the reactor

The CSTR was loaded with polywax 3000 as a start-up solvent. To be able to determine the amount of product accumulating in the reactor, the amount of solvent in the reactor has to be quantified. The liquid-phase product is collected intermittently, and this product contains both FT products and the polywax solvent. We can use the data about the amount of polywax remaining in the reactor as a function of time to estimate the residence time of the polywax (and thus any non-volatile liquid) in the reactor.

As the liquid is drained periodically, we need to consider the following thought process in order to relate the liquid residence time to the experimentally measured polywax fraction in the reactor as a function of time (see Fig. 4). Consider that at time $t = 0$, the reactor is loaded with 310 g of polywax and the FTS reaction commences. If A_1 grams of liquid sample is collected at time t_1, assuming that the total mass of liquid inside the reactor remains 310 g after sampling throughout the experiment, then the mass fraction of the polywax at time t_1 in the reactor, m_{p1}, is:

$$m_{p1} = \frac{310}{310 + A_2} \tag{7}$$

The mass of polywax removed from the reactor would be

$$M_{p,removed1} = m_{p1} \times A_1 \tag{8}$$

The mass of polywax remaining in the reactor at time t_1 after the sample has been collected would be:

$$M_{p1} = 310 - m_{p1} \times A_1 \tag{9}$$

For the next liquid sample, if A_2 gram of liquid is collected at time t_2, then the mass fraction of polywax in the reactor is:

$$m_{p2} = \frac{M_{p1}}{310 + A_2} \tag{10}$$

Therefore, the mass of polywax removed from the reactor would be

$$M_{p,removed2} = m_{p2} \times A_2 \tag{11}$$

Thus, the mass of polywax remaining in the reactor would be

$$M_{p2} = M_{p1} - m_{p2} \times a_2 \tag{12}$$

This calculation is repeated is for each sample taken at the various times.

Based on the experimentally measured mass and composition of the liquid sample collected for the experimental run, the mass fraction of polywax inside the reactor was calculated and is shown in Fig. 4.

Comparing with the hydrogen replacement rate in the gas phase which was around 6 h, it took roughly 900 h for the polywax fraction to get to 10% of the liquid inside the reactor. This signifies that the gas phase and the liquid phase have very different residence times.

If we assume that the vapor pressure of the polywax is very low, then it follows that there is no or very little polywax in the vapor phase. The unsteady state mass balance on the polywax in the reactor is given by:

$$V_L \frac{dm_p}{dt} = -Q_L m_p \tag{13}$$

where V_L is the volume of liquid inside the reactor; Q_L is the liquid flow out of the reactor; and m_p is the mass fraction of polywax in the liquid phase.

The average liquid residence time is defined as:

$$\tau_L \equiv \frac{V_L}{Q_L} \tag{14}$$

Substituting the residence time into Eq. (13) and integrating results in:

$$\ln\left(\frac{m_p}{m_{P0,0}}\right) = -\frac{1}{\tau_L}(t - t_0) \tag{15}$$

According to Eq. (15), the plot of the logarithm of the polywax mass fractions in the reactor versus time on stream should result in a straight line in which the slope is given by $-1/\tau_L$. To get a good estimate of the average residence time of the liquid, the data between 100 and 700 h were used and the results are presented in Fig. 5.

It can be seen from Fig. 5 that the log of the polywax mass fractions in the reactor versus time on stream is a straight line. The slope of the trend line is −0.003, which results in the average liquid-phase residence time of 333 h ≈ 13.9 days. This estimates the residence time of non-volatile liquid in the reactor. The residence time distribution presented in Fig. 5 also indicates that the reactor is well mixed and can be considered as an ideal slurry-phase CSTR.

These results show that as expected, there is a large difference between the residence time of the gas phase (1.87 h) and the non-volatile liquids in the reactor (333 h). This implies that it takes a long time for the liquid phase to reach steady state.

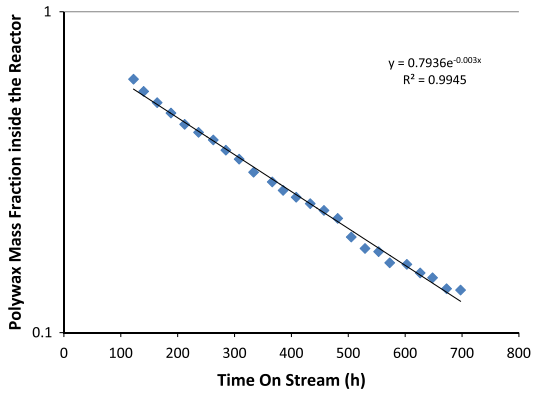

Fig. 5. Logarithm of the polywax mass fraction inside the reactor as a function of time on stream.

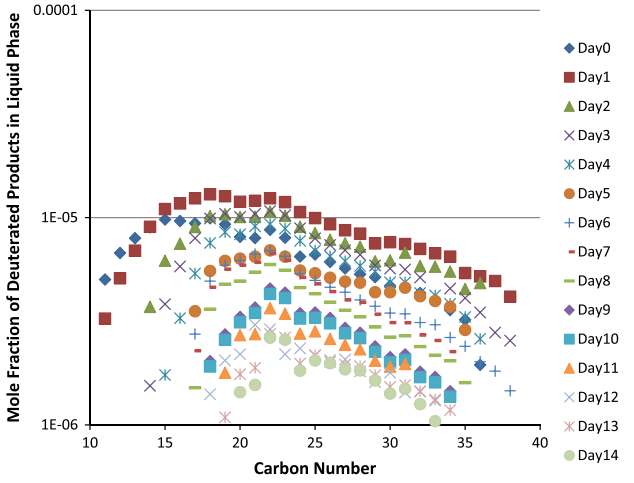

Fig. 6. Liquid-phase product distribution of deuterated products as a function of carbon number on different days on stream. Day 0 represents the end of D_2 tracing.

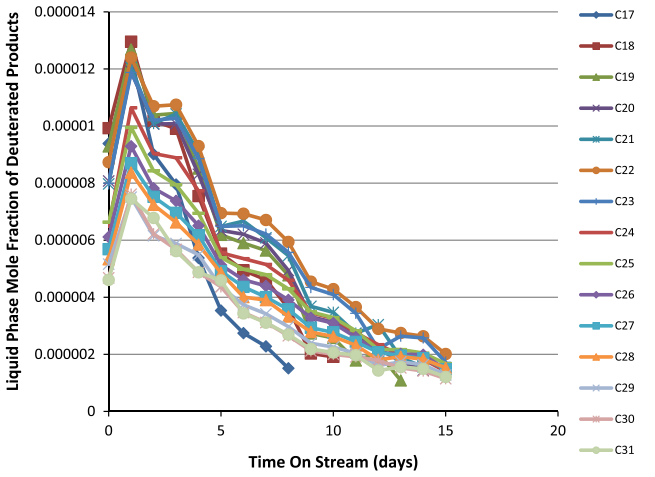

Fig. 7. Mole fraction of deuterated products in the liquid phase with time on stream. Day 0 represents the end of deuterium tracing.

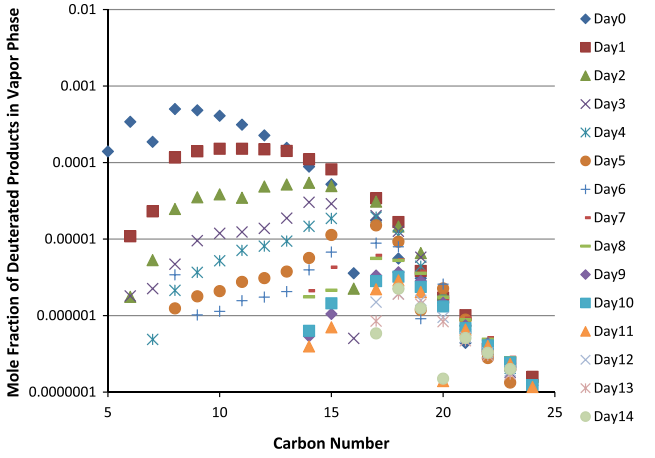

Fig. 8. The log of the mole fraction of deuterated products in the vapor phase plotted against length of hydrocarbon n distribution for different days. Day 0 represents the end of D_2 tracing.

6. Analysis of the liquid-phase product distribution

Based on the mass balance and the samples of the reactor wax collected daily, the composition of the slurry inside the reactor was determined and the liquid-phase product distribution is presented in Fig. 6.

The liquid-phase mole fractions can also be presented with time on stream for each carbon number as shown in Fig. 7.

The results in Figs. 6 and 7 show that the mole fraction of heavy products in the liquid phase is steadily decreasing while the mole fraction of lighter products drops quicker than the heavier products.

7. Analysis of the vapor-phase product distribution

The experimental setup is designed such that the vapor-phase products from the reactor can be collected and analyzed separately from the liquid-phase products. The log of the mole fraction of deuterated products in the vapor phase is plotted versus hydrocarbon length n for different days after the CO/D_2 feed was switched back to CO/H_2 in Fig. 8.

The measured change in vapor-phase mole fraction can also be plotted with time on stream for each carbon number as shown in Fig. 9.

The results in Figs. 8 and 9 show that the slope of the lighter products is changing with time on stream while the slope of the heavier products in the vapor phase is relatively constant. This suggests that the lighter products have a lower residence time, hence are being stripped out quicker than the heavier products.

8. The interaction of product accumulation with vapor–liquid equilibrium

The Fischer–Tropsch reaction has been known and used since the 1930s [1]. Despite being studied for over 80 years, the reaction is still not that well understood. We find different results from different researchers, different results for different catalysts. The results are complex and confusing. Perhaps, the complexity is not just due to the reaction mechanism. What if some of the complexity is caused by a combination of simple phenomena like vapor–liquid equilibrium (VLE) and product accumulation inside the reactor? The individual phenomena are quite simple. However, the interactions of these phenomena cause quite complex behavior. The question remains if this could occur in the FT reaction.

At vapor–liquid equilibrium, the partition coefficient or *K*-value is defined as:

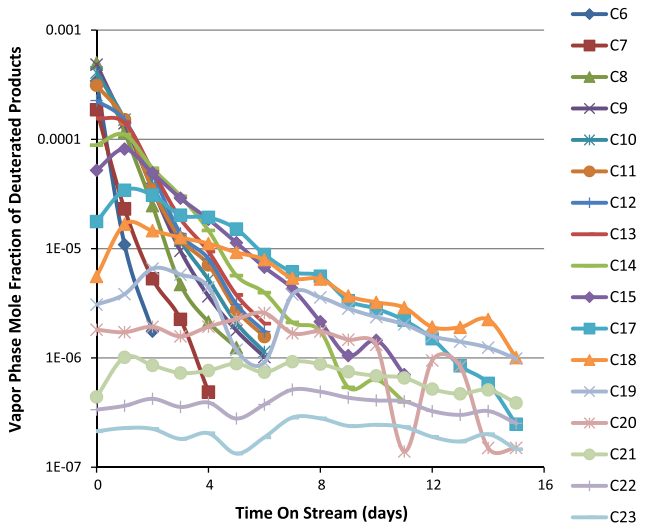

Fig. 9. Mole fraction of deuterated products in the vapor phase with time on stream. Day 0 represents the end of deuterium tracing.

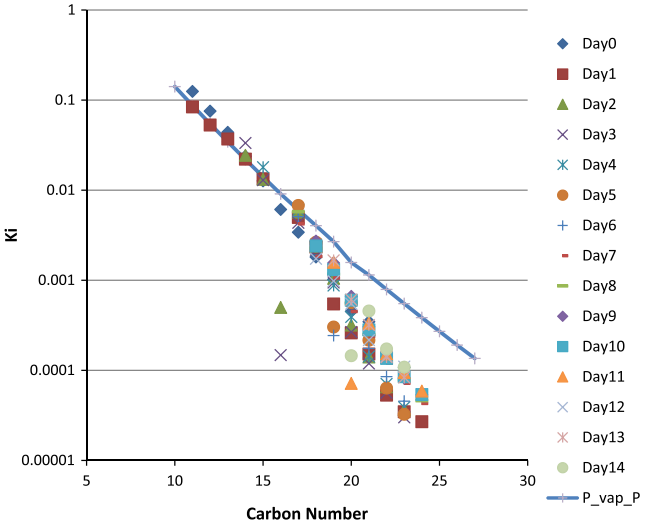

Fig. 10. The ratio of the mole fraction in the vapor phase to the mole fraction in the liquid phase ($K_n \equiv y_n/x_n$) with carbon number. Solid line is calculated from Raoult's law and is given by $P_{vap,n}/P$.

$$K_n \equiv \frac{y_n}{x_n} \tag{16}$$

where y_n is the mole fraction of species n in the vapor phase, and x_n is the mole fraction of species n in the liquid phase.

According to Raoult's law:

$$y_n P = x_n P_{vap,n} \tag{17}$$

where $P_{vap,}n$ is the vapor pressure of component n and P is the operating pressure.

This results in:

$$K_n = \frac{P_{vap,n}}{p} \tag{18}$$

Subsequently, the K-values calculated from the vapor pressure can be plotted and compared with the experimental results as shown in Fig. 10 to determine whether VLE is reached inside an FT reactor and to assess the impact of product accumulation on VLE. The vapor pressure data were obtained from *Yaws' Handbook of Antoine Coefficients for Vapor Pressure* (*2nd* Electronic Edition) [37].

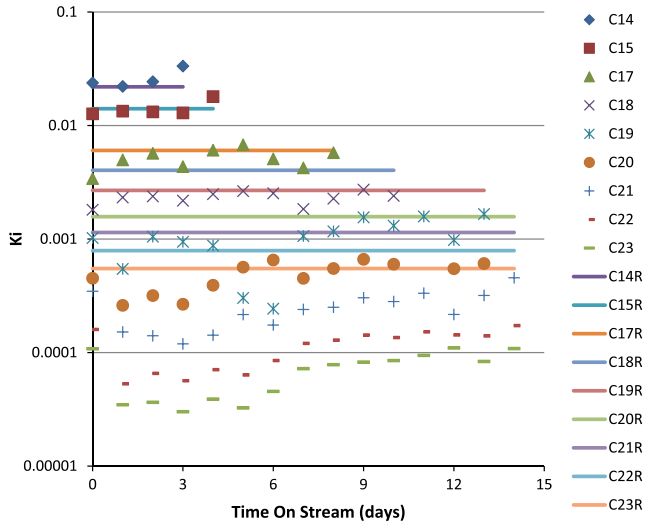

Fig. 11. Experimental K-values with time on stream for different carbon numbers compared to Raoult's law's predictions. Solid lines are calculated from Raoult's law and are given by $P_{vap,n}/P$.

The results in Fig. 10 show that vapor–liquid equilibrium is reached inside the FT reactor since the lighter hydrocarbons, up to around C_{17}, are accurately described by Raoult's law. The heavier hydrocarbons deviate from Raoult's law. Their vapor-phase mole fraction is lower than Raoult's law's predictions; alternatively, their liquid-phase mole fraction is higher than Raoult's law's predictions. This is because heavier hydrocarbons are preferentially retained inside the reactor because they have low diffusion coefficients and therefore do not have enough time to reach VLE. This would cause the measured K-values of heavier hydrocarbons to be less than predicted from Raoult's law. Thus, product accumulation affects VLE modeling. This suggests that some of the complexities in the FTS are caused by a combination of simple phenomena like product holdup and VLE.

The K-values can also be presented with time on stream as shown in Fig. 11, to assess how the experimental values change with time.

As before, the lighter products are accurately described by Raoult's law. However, Fig. 11 shows that the trends of heavier products tend toward the theoretical values albeit at a slow pace. This means that the higher the carbon number, the longer it takes to reach steady state.

9. Overall product distribution of deuterated products

It is generally assumed that the olefin readsorption probability increases with increasing carbon number due to increased residence times of longer chains in the liquid-filled pores of the catalyst. Chain length–dependent solubility [38–40] and chain length–dependent diffusivity [14,41,42] have been proposed as possible reasons.

Iglesia et al. [41] proposed that diffusion-limited removal of products from catalyst pellets can lead to enhanced readsorption and chain initiation by α-olefins, which reverses the chain termination steps that form these olefins and leads to heavier, more paraffinic products. Furthermore, they assert that exclusively diffusion-enhanced readsorption of olefins accounts for non-Schulz–Flory carbon number product distributions and decreasing

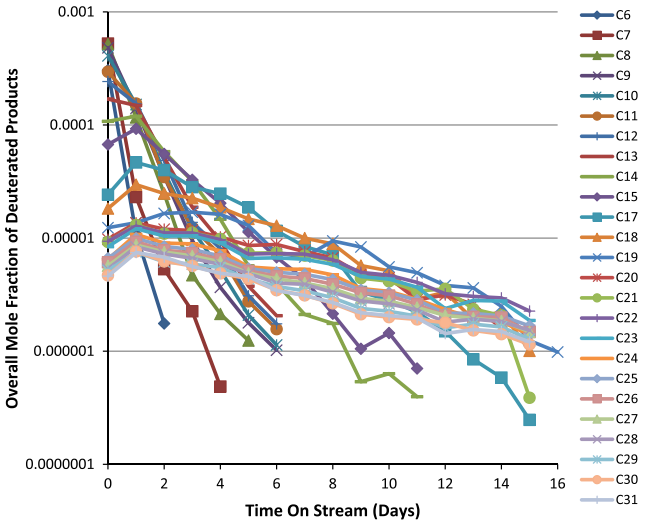

Fig. 12. Calculated mole fractions of total (vapor + liquid) deuterated products after introducing D_2 into the reactor. The D_2 is switched off and replace with H_2 at the end of Day 0.

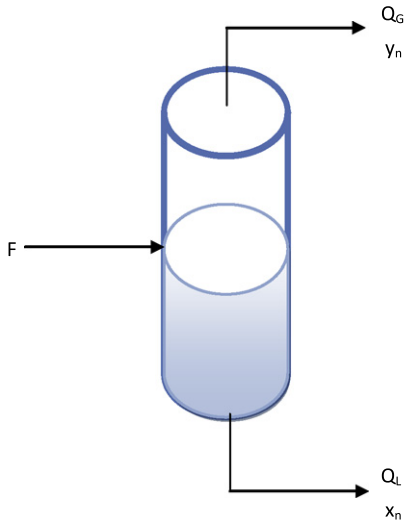

Fig. 13. Schematic diagram of the reactor as a stripping vessel for deuterated products. (F is the total molar flow of products, Q_G is the vapor molar flow, Q_L is the liquid molar flow, y_n is the mole fraction of component n in the vapor phase, and x_n is the mole fraction of component n in the liquid phase).

olefin contents with increasing carbon number observed during FT synthesis on cobalt and ruthenium catalysts.

In contrast to this, chain length–dependent contact time due to chain length–dependent solubility in the liquid product has been proposed earlier to cause the generally observed chain length dependences of olefin selectivities [38–40]. Kuipers et al. [17] showed that dissolution and physisorption can cause a much stronger chain length dependence than diffusion and would usually dominate.

To obtain more insight into the cause for chain length dependencies of secondary olefin reactions in FTS, the overall weight percent of deuterated hydrocarbon obtained after introducing D_2 into the reactor for 24 h is presented in Fig. 12.

The experimental results presented in Fig. 12 show that initially after the introduction of D_2/CO syngas, more lower-boiling deuterated products are formed when compared to the higher-boiling deuterated products. This is consistent with typical FT products which usually follow an ASF product distribution or a slight variation of it. It is worth noting that after the syngas has been switched back to H_2/CO at TOS = 24 h, the percentage of lower-boiling deuterated products drops more quickly than the higher-boiling deuterated products. Some of the higher-boiling deuterated compounds appear to be increasing in concentration for up to 50 h after the deuterium has been switched off. Although the amount of the heavier product in the reactor is changing slowly, the lighter ones are changing very fast, and thus, the observed increase in mole fraction of the heavier ones is due to stripping of the lighter components and not making heavier ones. This means that the lower molecular weight products exit the reactor very quickly, and the labeled fraction of these lower molecular weight products will be little affected by accumulation. On the other hand, the average residence time will increase with carbon number and the higher carbon number products may be affected by accumulation of unlabeled products.

Schulz and Claeys [43] estimated average residence times of certain product molecules C_2–C_{11} in CSTR system by the ratio of the actual number of moles of a compound to the total molar exit flow rate of this compound. Their results showed strongly increasing residence times of product compounds with carbon number, which signified that chain length–dependent solubility can affect residence times of products and thereby the extent of secondary olefin reactions. They never measured the residence time of heavier products. To calculate the residence time of heavier products, we compute an unsteady state mass balance on the deuterated products inside the reactor.

10. Unsteady state mass balance on the deuterated products inside the reactor

After the feed gas has been changed from CO/D_2 back to CO/H_2, the reactor can be considered as a vessel in which deuterated products are being stripped out and removed in the vapor phase by the gas stream and removed in the liquid phase by flow as illustrated in Fig. 13. We assume that the reactor is well mixed such that the mole fraction of component n in the vapor/liquid removed from the reactor at some time t is the same as the mole fraction of that component in the vapor/liquid phase in the reactor.

If we ignore the effects of reacting products (olefin reactivity) on the products modeling, then the unsteady state mass balance on component n can be written as:

$$V_G C_G \frac{dy_n}{dt} + V_L C_L \frac{dx_n}{dt} = -Q_L C_L x_n - Q_G C_G y_n \tag{19}$$

where V_G is the volume of gas/vapor inside the reactor; V_L, the volume of liquid inside the reactor; C_G, the molar concentration of both the vapor product stream and the vapor inside the reactor; C_L, the molar concentration of both the liquid inside the reactor and the liquid stream product stream; Q_G, the vapor molar flow rate out of the reactor; Q_L, the liquid molar flow rate out of the reactor; y_n, the mole fraction of component n in the vapor phase in both the reactor and the vapor product leaving the reactor; and x_n is the mole fraction of component n in the liquid phase in both the reactor as well as the liquid product removed from the reactor.

Assuming that the vapor and the liquid are in equilibrium then

$$y_n = K_n x_n \tag{20}$$

Thus, Eq. (19) becomes:

$$\frac{dx_n}{dt} = -\frac{(Q_G C_G K_n + Q_L C_L)}{(V_G C_G K_n + V_L C_L)} x_n \tag{21}$$

Alternatively,

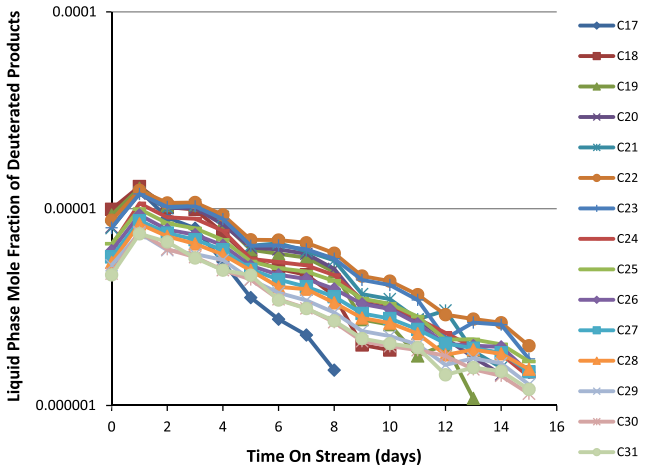

Fig. 14. The log of mole fraction of deuterated products in the liquid phase with time on stream. The slope of each line represents the inverse of the residence time of that product in the reactor.

$$\frac{dy_n}{dt} = -\frac{\left(Q_C C_G + \frac{Q_L C_L}{K_n}\right)}{\left(V_G C_G + \frac{V_L C_L}{K_n}\right)} y_n \tag{22}$$

Hence, we defined the mean residence time of each product to be the inverse of the slopes of Eqs. (21) and (22).

10.1. For heavier hydrocarbons, with a low vapor pressure $K_n \ll 1$

For hydrocarbons which are relatively involatile, Eq. (21) reduces to:

$$\frac{dx_n}{dt} = -\frac{Q_L}{V_L} x_n = -\frac{1}{\tau_L} x_n \tag{23}$$

Integrating both sides results in:

$$\ln\left(\frac{x_n}{x_{n,0}}\right) = -\frac{1}{\tau_L}(t - t_0) \tag{24}$$

Thus, for the heavier hydrocarbons, the main mode of removal from the reactor is through the liquid flow, and these hydrocarbons will have the same residence time as the liquid. We can plot the logarithm of the mole fraction of the deuterated hydrocarbon n in the liquid phase, x_n, versus time, where the slope of the line is the inverse of the average residence time in the liquid for that hydrocarbon. The measured change in liquid-phase mole fraction with time is presented in Fig. 14.

The slopes of the mole fractions with time for the carbon numbers shown in Fig. 14 were calculated. Assuming that each slope is given by $-1/\tau_{n,L}$ provides a method for calculating the residence time of each carbon number.

10.2. For lighter hydrocarbons, with a high vapor pressure $K_n \gg 1$

For hydrocarbons which are relatively insoluble, Eq. (22) reduces to:

$$\frac{dy_n}{dt} = -\frac{Q_G}{V_G} y_n = -\frac{1}{\tau_G} y_n \tag{25}$$

Integrating both sides results in:

$$\ln\left(\frac{y_n}{y_{n,0}}\right) = -\frac{1}{\tau_L}(t - t_0) \tag{26}$$

Thus, for the lighter hydrocarbons, the main mode of removal from the reactor is through the gas flow or stripping, and these hydrocarbons will have the same residence time as the gas/vapor. We can plot the logarithm of the mole fraction of the deuterated hydrocarbon n in the vapor phase, y_n, versus time, where the slope of the line is the inverse of the average residence time in the vapor for that hydrocarbon. The measured change in vapor-phase mole fraction with time is presented in Fig. 15.

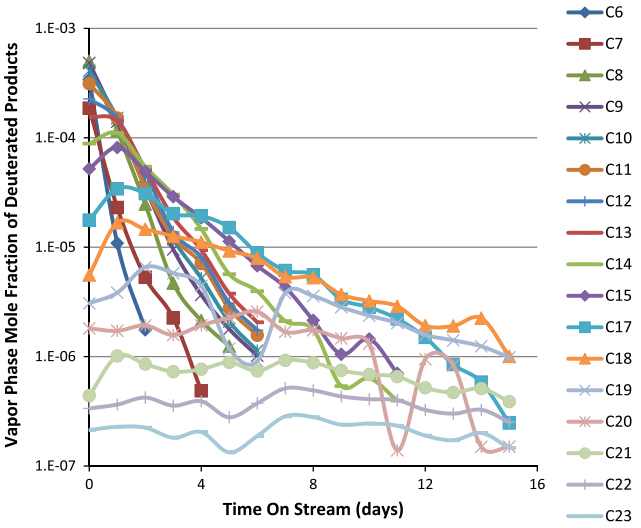

Fig. 15. The log of mole fraction of deuterated products in the vapor phase with time on stream. The slope of each line represents the inverse of the residence time of that product in the reactor.

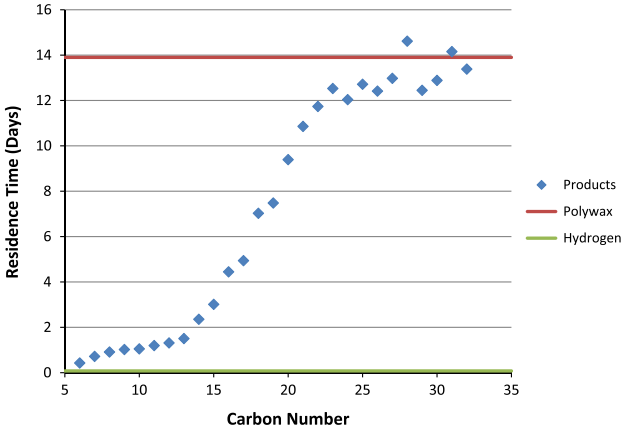

Fig. 16. The average residence time with carbon number for products inside a reactor calculated from the slopes of the curves in Figs. 12 and 13.

The average residence times of products with carbon number 16 and higher were calculated from the liquid-phase slopes. The residence time of products lighter than C_{16} were calculated from the vapor-phase slopes. The overall results of the residence time of the hydrocarbons versus chain length are presented in Fig. 16.

The results presented in Fig. 16 show that the residence time increases with carbon number up to C_{22}, and products with chain length 22 and higher have the same residence time as the non-volatile polywax. This implies that the major removal method for products C_{22} and heavier is the liquid-phase flow because these products have low vapor pressures. Therefore, the stripping by the vapor flow is not a major method of removal for these products. The major removal method for products lighter than C_{10} is the gas phase. These products will have a similar residence time as the highly volatile/insoluble component. The products with chain length between 10 and 22 are removed by both the vapor flow and the liquid flow as can be seen by their average residence time being higher than the gas-phase residence time but less than

the average residence time of the non-volatile liquid. The lighter products would be expected to be in vapor–liquid equilibrium more quickly than the higher molecular weight products.

These results confirm that the lower molecular weight products have a lower residence time than the longer chain products (i.e., tend to the residence time of the insoluble gas), and the fraction of these lower molecular weight products will be little affected by accumulation in the liquid phase/reactor. The results also imply that the lighter products will reach steady state quicker than the heavier products.

11. Conclusions

The average residence time of the highly-volatile/insoluble gas is around 1.87 h, while the non-volatile liquid has an average residence time of around 13.9 days. The lower molecular weight products exit the reactor very quickly, and the fraction of these lower molecular weight products will be little affected by accumulation as their residence time approaches that of the gas phase. The average residence time increases with carbon number, and the higher carbon number products have a longer residence time in the reactor as their residence time approaches that of the non-volatile polywax. These products will be more affected by accumulation in the liquid phase and hence will take longer to reach equilibrium. The results show that products with a chain length of 22 and higher have the same residence time as the liquid. If it takes 3–4 residence times to reach steady state, then it would take around 2 months to fully reach the steady state for these products in an FT reactor.

Vapor–liquid equilibrium plays an important role in modeling the behavior of an FT reactor. The results show that vapor–liquid equilibrium is reached inside an FT reactor for components up to around C_{17}. This suggests that chain length–dependent solubility in the liquid phase is the predominant cause for chain length dependencies of secondary olefin reactions in Fischer–Tropsch synthesis, and diffusion-limited removal of products is only significant for products with carbon number greater than 17.

The results obtained suggest that Raoult's law sufficiently describe VLE in a Fischer–Tropsch reactor. The preferential holdup of heavier products in the reactor affects the VLE modeling. Thus, some of the complexities in the FTS are caused by a combination of simple phenomena (e.g., product holdup and VLE). The interactions of these phenomena cause quite complex behavior.

References

[1] D.F. Smith, C.O. Hawk, P.L. Golden, The mechanism of the formation of higher hydrocarbons from water gas, J. Am. Chem. Soc. 52 (1930) 3221–3232.
[2] R.A. Friedel, R.B. Anderson, Composition of synthetic liquid fuels. I. Product distribution and analysis of C_5–C_8 paraffin isomers from cobalt catalyst, J. Am. Chem. Soc. 72 (1950) 1212–1215.
[3] J.T. Kummer, H.H. Podgurski, W.B. Spencer, P.H. Emmett, Mechanism studies of the Fischer–Tropsch synthesis. The addition of radioactive alcohol, J. Am. Chem. Soc. 73 (1951) 564–569.
[4] W. Keith Hall, R.J. Kokes, P.H. Emmett, Mechanism studies of the Fischer–Tropsch synthesis, the addition of radioactive methanol, carbon dioxide and gaseous formaldehyde, J. Am. Chem. Soc. 79 (1957) 2983–2989.
[5] W. Keith Hall, R.J. Kokes, P.H. Emmett, Mechanism studies of the Fischer–Tropsch synthesis: the incorporation of radioactive ethylene, propionaldehyde and propanol, J. Am. Chem. Soc. 82 (1960) 1027–1037.
[6] G. Henrici-Olive, S. Olive, The Fischer–Tropsch synthesis: molecular weight distribution of primary products and reaction mechanism, Angew. Chem. Int. Ed. Engl. 15 (1976) 136–141.
[7] C.N. Satterfield, G.A. Huff, Carbon number distribution of Fischer–Tropsch products formed on an iron catalyst in a slurry reactor, J. Catal. 73 (1982) 187–197.
[8] C.N. Satterfield, G.A. Huff, J.P. Longwell, Product distribution from iron catalysts in Fischer–Tropsch slurry reactors, Ind. Eng. Chem. Process. Des. Dev. 21 (1982) 465–470.
[9] R.A. Dictor, A.T. Bell, An explanation for deviations of Fischer–Tropsch products from a Schulz–Flory distribution, Ind. Eng. Chem. Process. Des. Dev. 22 (1983) 678–681.
[10] R.B. Anderson, in: P.H. Emmett (Ed.), Catalysis, vol. 4, Reinhold, New York, 1956, pp. 123–163.
[11] H.E. Atwood, C.O. Bennett, Kinetics of the Fischer–Tropsch reaction over iron, Ind. Eng. Chem. Process. Des. Dev. 18 (1979) 163–170.
[12] R.J. Madon, W.F. Taylor, Fischer–Tropsch synthesis on a precipitated iron catalyst, J. Catal. 69 (1981) 32–43.
[13] G.A. Huff, C.N. Satterfield, Evidence for two chain growth probabilities on iron catalysts in the Fischer–Tropsch synthesis, J. Catal. 85 (1984) 370–379.
[14] E. Iglesia, S.C. Reyes, R.J. Madon, Transport-enhanced α-olefin readsorption pathways in Ru-catalyzed hydrocarbon synthesis, J. Catal. 129 (1991) 238–256.
[15] E.W. Kuipers, C. Scheper, J.H. Wilson, I.H. Vinkenburg, H. Oosterbeek, Non-ASF product distributions due to secondary reactions during Fischer–Tropsch synthesis, J. Catal. 158 (1996) 288–300.
[16] T. Komaya, A.T. Bell, Estimates of rate coefficients for elementary processes occurring during Fischer–Tropsch synthesis over Ru/TiO_2, J. Catal. 146 (1994) 237–248.
[17] E.W. Kuipers, I.H. Vinkenburg, H. Oosterbeek, Chain length dependence of α-olefin readsorption in Fischer–Tropsch synthesis, J. Catal. 152 (1995) 137–146.
[18] L.–M. Tau, H.A. Dabbagh, B.H. Davis, Fischer–Tropsch synthesis: comparison of carbon-14 distributions when labeled alcohol is added to the synthesis gas, Energy Fuels 5 (1991) 174–179.
[19] L.–M. Tau, H.A. Dabbagh, B. Chawla, B.H. Davis, Fischer–Tropsch synthesis with an iron catalyst: incorporation of ethene into higher carbon number alkanes, Catal. Lett. 7 (1990) 141–149.
[20] L.–M. Tau, H.A. Dabbagh, S. Bao, B.H. Davis, Fischer–Tropsch synthesis. Evidence for two chain growth mechanisms, Catal. Lett. 7 (1990) 127–140.
[21] K.R. Krishna, A.T. Bell, The role of C_2 intermediates in Fischer–Tropsch synthesis over ruthenium, Catal. Lett. 14 (1992) 305–313.
[22] R.J. Madon, E. Iglesia, The importance of olefin readsorption and H_2/CO reactant ratio for hydrocarbon chain growth on ruthenium catalysts, J. Catal. 139 (1993) 576–590.
[23] R.J. Madon, S.C. Reyes, E. Iglesia, Primary and secondary reaction pathways in ruthenium-catalyzed hydrocarbon synthesis, J. Phys. Chem. 95 (1991) 7795–7804.
[24] G.P. van der Laan, A.A.C.M. Beenackers, Hydrocarbon selectivity model for the gas–solid Fischer–Tropsch synthesis on precipitated iron catalysts, Ind. Eng. Chem. Res. 38 (1999) 1277–1290.
[25] X. Zhan, B.H. Davis, Two alpha Fischer–Tropsch product distribution. A role for vapor–liquid equilibrium?, Petrol Sci. Technol. 18 (2000) 1037–1053.
[26] A.P. Raje, B.H. Davis, Effect of vapor–liquid equilibrium on Fischer–Tropsch hydrocarbon selectivity for a deactivating catalyst in a slurry reactor, Energy Fuels 10 (1996) 552–560.
[27] B. Shi, B.H. Davis, Fischer–Tropsch synthesis: accounting for chain length related phenomena, Appl. Catal. A: Gen. 277 (2004) 61–69.
[28] J.T. Kummer, T.W. Dewitt, P.H. Emmett, Some mechanism studies on the Fischer–Tropsch synthesis using C14, J. Am. Chem. Soc. 70 (1948) 3632–3643.
[29] J.T. Kummer, P.H. Emmett, Fischer–Tropsch synthesis mechanism studies. The addition of radioactive alcohols to the synthesis gas, J. Am. Chem. Soc. 75 (1953) 5177–5183.
[30] G. Blyholder, P.H. Emmett, Fischer–Tropsch synthesis mechanism studies. The addition of radioactive ketene to the synthesis gas, J. Phys. Chem. 63 (1959) 962–965.
[31] G. Blyholder, P.H. Emmett, Fischer–Tropsch synthesis mechanism studies. II. The addition of radioactive ketene to the synthesis gas, J. Phys. Chem. 64 (1960) 470–472.
[32] P.M. Maitlis, H.C. Long, R. Quyoum, M.L. Turner, Z.–Q. Wang, Heterogeneous catalysis of C–C bond formation: black art or organometallic science?, Chem Commun. (1996) 1–8.
[33] M.L. Turner, H.C. Long, A. Shenton, P.K. Byers, P.M. Maitlis, The alkenyl mechanism for Fischer–Tropsch surface methylene polymerisation; the reactions of vinylic probes with CO/H_2, over rhodium catalysts, Chem. Eur. J. 1 (1995) 549–556.
[34] A. Raje, B.H. Davis, in: J.J. Spring (Ed.), Fischer–Tropsch synthesis. Mechanism studies using isotope catalysis, vol. 12, The Royal Chem. Soc., Cambridge, 1996, p. 52.
[35] B. Shi, R.J. O'Brien, S. Bao, B.H. Davis, Mechanism of the isomerization of 1-alkene during iron-catalyzed Fischer–Tropsch synthesis, J. Catal. 199 (2001) 202–208.
[36] B. Shi, B.H. Davis, ^{13}C-tracer study of the Fischer–Tropsch synthesis: another interpretation, Catal. Today 58 (2000) 255–261.
[37] C.L. Yaws, P.K. Narasimhan, C. Gabbula, Yaws' Handbook of Antoine Coefficients for Vapor Pressure, Knovel, 2nd Electronic ed., 2009 (accessed on 08.30.10).
[38] R. Dictor, A.T. Bell, Fischer–Tropsch synthesis over reduced and unreduced iron oxide catalysts, J. Catal. 97 (1986) 121–136.
[39] R. Dictor, A.T. Bell, Studies of Fischer–Tropsch synthesis over a fused iron catalyst, Appl. Catal. 20 (1986) 145–162.
[40] L.-M. Tau, H.A. Dabbagh, B.H. Davis, Fischer–Tropsch synthesis: ^{14}C tracer study of alkene incorporation, Energy Fuels 4 (1990) 94–99.
[41] E. Iglesia, S.C. Reyes, R.J. Madon, S.L. Soled, Selectivity control and catalyst design in the Fischer–Tropsch synthesis: sites. Pellets, and reactors, Adv. Catal. 39 (1993) 221–302.
[42] R.J. Madon, E. Iglesia, Hydrogen and CO intrapellet diffusion effects in ruthenium-catalyzed hydrocarbon synthesis, J. Catal. 149 (1994) 428–437.
[43] H. Schulz, M. Claeys, Reactions of α-olefins of different chain length added during Fischer–Tropsch synthesis on a cobalt catalyst in a slurry reactor, Appl. Catal. A: Gen. 186 (1999) 71–90.